

## Article

# Recyclable Carbon Cloth-Supported ZnO@Ag<sub>3</sub>PO<sub>4</sub> Core–Shell Structure for Photocatalytic Degradation of Organic Dye

Yuan Yi <sup>1</sup>, Qifang Guan <sup>1</sup>, Wenguang Wang <sup>1,\*</sup>, Siyuan Jian <sup>1</sup>, Hengchao Li <sup>1</sup>, Liangpeng Wu <sup>2</sup>, Haiyan Zhang <sup>1</sup> and Chuanjia Jiang <sup>3,\*</sup>

<sup>1</sup> School of Materials and Energy, Guangdong University of Technology, Guangzhou Higher Education Mega Center 100#, Guangzhou 510006, China

<sup>2</sup> Advanced Energy Science and Technology Guangdong Laboratory, Huizhou 516000, China

<sup>3</sup> College of Environmental Science and Engineering, Nankai University, 38 Tongyan Rd., Tianjin 300350, China

\* Correspondence: wenguangwang2005@163.com (W.W.); jiangcj@nankai.edu.cn (C.J.)

**Abstract:** The extensive use of organic dyes in industry has caused serious environmental problems, and photocatalysis is a potential solution to water pollution by organic dyes. The practical application of powdery photocatalysts is usually limited by the rapid recombination of charge carriers and difficulty in recycling. In this study, recyclable carbon cloth-supported ZnO@Ag<sub>3</sub>PO<sub>4</sub> composite with a core–shell structure was successfully prepared by solvothermal treatment and subsequent impregnation–deposition. The as-prepared carbon cloth-supported ZnO@Ag<sub>3</sub>PO<sub>4</sub> composite showed an improved photocatalytic activity and stability for the degradation of rhodamine B (RhB), a model organic dye, under visible light irradiation. The decomposition ratio of RhB reached 87.1% after exposure to visible light for 100 min, corresponding to a reaction rate constant that was 4.8 and 15.9 times that of carbon cloth-supported Ag<sub>3</sub>PO<sub>4</sub> or ZnO alone. The enhanced performance of the composite can be attributed to the effectively inhibited recombination of photoinduced electron–hole pairs by the S-scheme heterojunction. The carbon fibers further promoted the transfer of charges. Moreover, the carbon cloth-supported ZnO@Ag<sub>3</sub>PO<sub>4</sub> can be easily separated from the solution and repeatedly used, demonstrating a fair recyclability and potential in practical applications.

**Keywords:** carbon cloth; silver phosphate; zinc oxide; S-scheme heterojunction; wastewater treatment



**Citation:** Yi, Y.; Guan, Q.; Wang, W.; Jian, S.; Li, H.; Wu, L.; Zhang, H.; Jiang, C. Recyclable Carbon Cloth-Supported ZnO@Ag<sub>3</sub>PO<sub>4</sub> Core–Shell Structure for Photocatalytic Degradation of Organic Dye. *Toxics* **2023**, *11*, 70. <https://doi.org/10.3390/toxics11010070>

Academic Editor: Tiziana Missana

Received: 28 December 2022

Revised: 7 January 2023

Accepted: 8 January 2023

Published: 11 January 2023



**Copyright:** © 2023 by the authors. Licensee MDPI, Basel, Switzerland. This article is an open access article distributed under the terms and conditions of the Creative Commons Attribution (CC BY) license (<https://creativecommons.org/licenses/by/4.0/>).

## 1. Introduction

With the rapid development of the textile and dyeing industry, large quantities of organic dye-laden wastewater have been discharged into the natural waters, causing a range of environmental problems. Many of the organic dyes are toxic to human health or aquatic life [1,2]. Over the past decades, various destructive and nondestructive techniques have been explored for removing organic dyes from wastewater, including adsorption, filtration, biodegradation, advanced oxidation processes, photocatalysis, etc. [3–6]. Amongst these approaches, semiconductor-based photocatalysis can degrade and detoxify organic pollutants, including dyes, utilizing inexhaustible solar energy, which is expected to solve the problems of increasingly serious water pollution by organic dyes [7–10].

Zinc oxide (ZnO) is a versatile semiconductor photocatalysts with high ultraviolet (UV) shielding and refractive index, high electron mobility, and strong luminescence at room temperature [11], and ZnO-based photocatalysis has been widely explored for removing wastewater pollutants, including organic dyes [12–14]. However, as a typical broad-bandgap semiconductor, ZnO can be mainly excited by UV light, resulting in a low utilization rate of the visible light fraction of solar radiation, which, together with its vulnerability to corrosion under both irradiated and dark conditions [15,16], hinders the large-scale application of pure ZnO-based materials in the field of environmental photocatalysis [17]. The coupling of two band-matched semiconductors to form a heterojunction is an effective way to reduce the recombination of photoelectron–hole pairs and improve

the performance of photocatalytic materials [18,19]. Moreover, the coating of a material less prone to corrosion onto the surface of ZnO can dramatically enhance the stability of ZnO-based photocatalysts [15,20]. Since Ye et al. reported the use of silver phosphate ( $\text{Ag}_3\text{PO}_4$ ) in water oxidation and organic contaminant decomposition,  $\text{Ag}_3\text{PO}_4$ , a visible light-responsive semiconductor, has been widely considered as a promising material for solar photocatalysis [21–23]. Despite its low solubility in water, however, we have previously observed that, during extended photocatalytic tests, photoelectrons can induce the precipitation of metallic Ag films on the surface of  $\text{Ag}_3\text{PO}_4$ , which shield light and lead to the deactivation of  $\text{Ag}_3\text{PO}_4$  [24]. It has been demonstrated that the combination of ZnO with  $\text{Ag}_3\text{PO}_4$  could improve the photocatalytic activity of ZnO/ $\text{Ag}_3\text{PO}_4$  [25–27], though an improvement in performance stability is less straightforward, with contradicting results reported [25,28].

Up to now, a majority of the reported photocatalysts exist in the state of powder, which causes difficulty in separation and recycling when it comes to practical applications [29,30], highlighting the need for preparing immobilized photocatalysts with both high activity and recyclability [31]. Carbon cloth has unique physical and chemical properties such as a large specific surface area, excellent electrical conductivity, high strength, good thermal stability, and good corrosion resistance, which has been widely used in supercapacitors, lithium-ion batteries, electrocatalysis, microwave absorption, and other fields [32–34]. It was reported in our previous work that using carbon cloth as the catalyst support can effectively improve the photocatalytic performance and recyclability of the photocatalyst [35]. Thus, it is hypothesized that loading composites of ZnO and  $\text{Ag}_3\text{PO}_4$  with well-designed structures onto carbon cloth may yield a recyclable photocatalyst with high activity.

In this work, we reported the synthesis of a hybrid ZnO@ $\text{Ag}_3\text{PO}_4$  core-shell structure grown on carbon cloth via a calcination treatment followed by a two-step solution route (including a solvothermal treatment and subsequent impregnation-deposition) and evaluated its performance for the photocatalytic degradation of rhodamine B (RhB), a widely used organic dye known to be toxic to both humans and aquatic life [1,36]. The ZnO@ $\text{Ag}_3\text{PO}_4$  heterostructure is conducive to photocatalytic activity improvement under visible light irradiation, whereas the carbon fibers, as high-speed electron transfer channels, are also beneficial to charge separation. As a result, the carbon cloth-supported ZnO@ $\text{Ag}_3\text{PO}_4$  composite material exhibits a dramatic visible light photocatalytic activity compared with that of carbon cloth-supported ZnO and  $\text{Ag}_3\text{PO}_4$ . Additionally, the free-standing carbon cloth-supported ZnO@ $\text{Ag}_3\text{PO}_4$  can be easily withdrawn from a simulated wastewater solution and reused, which makes it a recyclable photocatalyst with potential for practical applications.

## 2. Materials and Methods

The procedures for synthesizing the materials are illustrated in Figure 1.

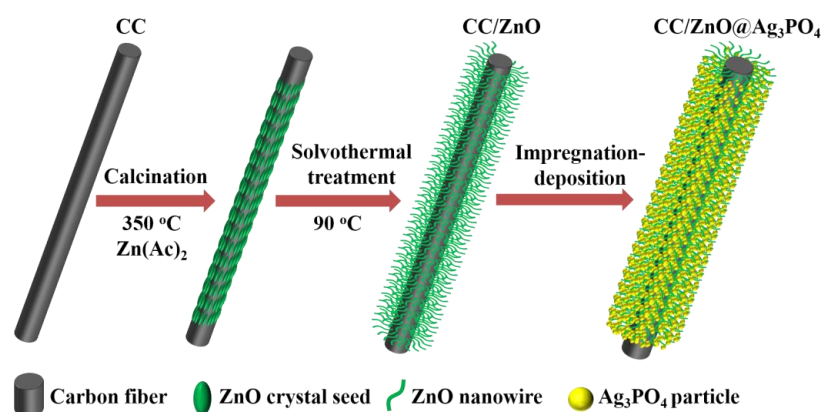


**Figure 1.** Schematic illustration for the synthesis procedure of the carbon cloth-supported ZnO and ZnO@ $\text{Ag}_3\text{PO}_4$  composite.

### 2.1. Deposition of ZnO Crystal Seeds on Carbon Cloth

The carbon cloth (WOS: 1009-17070602, average thickness: 0.33 mm, and nominal basic weight: 115.0 g/m<sup>2</sup>) with dimensions of 2 cm × 2 cm was successively dipped into acetone, anhydrous ethanol, and deionized water for 20 min in ultrasonic bath to remove the surface impurities. Then, the carbon cloth was soaked in nitric acid (65%) for 24 h to improve the surface hydrophilicity. After that, the carbon cloth was cleaned with deionized water several times and dried in an oven at 60 °C for 12 h.

ZnO crystal seeds were deposited on the carbon cloth by the calcination method. Specifically, 0.18 mmol of anhydrous zinc acetate was completely dissolved in 30 mL of anhydrous ethanol under continuous magnetic stirring. Afterwards, the mixed solution was slowly dripped onto the pretreated carbon cloth, and the obtained wet carbon cloth was further heated in a muffle furnace at 350 °C for 20 min in air. After cooling to room temperature, white ZnO crystal seeds could be found to adhere to the surfaces of carbon fibers.

### 2.2. Growth of ZnO Nanowires on Carbon Cloth

ZnO nanowires were grown on carbon cloth by a simple solvothermal method. Firstly, 3 mmol of zinc nitrate hexahydrate (Zn(NO<sub>3</sub>)<sub>2</sub>·6H<sub>2</sub>O) and 2 mmol of hexamethylenetetramine (HMTA) were dissolved in a certain volume of mixed solution containing aqueous ammonia (3 mL) and deionized water (70 mL), followed by being poured into a 100 mL autoclave with Teflon liner. Subsequently, the carbon cloth with ZnO crystal seeds was vertically soaked into the solution, and then, the autoclave was sealed and heated at 90 °C for 24 h. After the reaction, the autoclave naturally cooled down to room temperature. Finally, the carbon cloth with ZnO nanowires (denoted as CC/ZnO) was removed from the autoclave and washed with deionized water and ethanol several times and dried in an oven at 60 °C overnight.

### 2.3. Preparation of Carbon Cloth-Supported ZnO@Ag<sub>3</sub>PO<sub>4</sub> Composite

The carbon cloth-supported ZnO@Ag<sub>3</sub>PO<sub>4</sub> composite was prepared by a simple impregnation–deposition method. The whole experiment process was carried out in dark conditions to avoid undesired photo corrosion. A certain amount of AgNO<sub>3</sub> and (NH<sub>4</sub>)<sub>2</sub>HPO<sub>4</sub> were separately dissolved in deionized water to form solutions with concentrations of 0.5 and 0.17 mol/L, respectively. Then, the as-prepared carbon cloth-supported ZnO was soaked in AgNO<sub>3</sub> solution for 6 h. After that, the wet AgNO<sub>3</sub>-infiltrated CC/ZnO was taken out and immersed in (NH<sub>4</sub>)<sub>2</sub>HPO<sub>4</sub> solution for 1 min and then was again dipped back into the AgNO<sub>3</sub> solution. This soaking process was repeated 20 times. Finally, the obtained carbon cloth-supported ZnO@Ag<sub>3</sub>PO<sub>4</sub> composite (denoted as CC/ZnO@Ag<sub>3</sub>PO<sub>4</sub>) was washed with deionized water and dried at 60 °C for 12 h. For comparison, carbon cloth-supported Ag<sub>3</sub>PO<sub>4</sub> (denoted as CC/Ag<sub>3</sub>PO<sub>4</sub>) was also prepared by directly soaking pure carbon cloth into the precursor solutions in the same way as described above.

### 2.4. Characterization

The morphological observation of the carbon cloth-supported photocatalysts was accomplished on a SU8010 field emission scanning electron microscope (FESEM, Hitachi, Japan) and a JEM2010F transmission electron microscope (TEM, JEOL, Japan). The crystal structure and phase composition of the samples were analyzed by a D/MAX-Ultima IV X-ray diffractometer (XRD, Rigaku, Japan) using Cu K $\alpha$  radiation with a scanning rate of 8°/min. X-ray photoelectron spectroscopy (XPS) was measured on an EscaLab 250Xi electron spectrometer (Thermo, Waltham, MA, USA) excited by using Al K $\alpha$  radiation. UV–Vis diffuse reflectance spectra (DRS) of the samples were recorded on a UV9000 UV–Vis spectrophotometer (Metash, Shanghai, China), with BaSO<sub>4</sub> used as a reflectance standard.

### 2.5. Photocatalytic Activity Measurement

The photocatalytic activities of the carbon cloth-supported photocatalysts were evaluated by the degradation of RhB ( $1.0 \times 10^{-5}$  mol/L) as the target organic pollutant at room temperature, and a LED lamp with a fixed wavelength of 420 nm was used as the visible light source to trigger the reaction. To be more specific, a piece of carbon cloth-supported photocatalyst (2 cm  $\times$  2 cm) was vertically placed into a beaker containing 60 mL of RhB solution. Before turning on the LED light, the catalytic reaction system was magnetically stirred in dark for 30 min to reach adsorption equilibrium. During the process of light irradiation, aliquots of the supernatant were removed with a disposable dropper at regular time intervals and transfused into a colorimeter cell. The absorbance of the solution was measured by a UV–visible spectrophotometer, and the activities of the photocatalysts were estimated by comparing the apparent reaction rate constant, which can be calculated by  $\ln(C_0/C_t) = kt$ . In this equation,  $C_0$  and  $C_t$  represent the concentration of RhB solution initially at the adsorption equilibrium (before the light was turned on) and at the reaction time of  $t$ , respectively, where  $k$  represents the reaction rate constant, and  $t$  represents the irradiation time.

## 3. Results and Discussion

### 3.1. Phase Structure

The crystal structure and phase composition of the samples were characterized by XRD, and the related patterns are shown in Figure 2. The pure carbon cloth (CC) exhibits a relatively wide diffraction peak at  $26^\circ$ , corresponding to the (002) plane of the carbon fiber [37]. In the case of CC/ZnO, besides the weak peak of carbon cloth, many new diffraction peaks (labeled with  $\blacklozenge$ ) appear in the XRD pattern, including three strong peaks at  $31.7^\circ$ ,  $34.4^\circ$ , and  $36.3^\circ$ , which can be assigned to the (100), (002), and (101) planes of the hexagonal ZnO (JCPDS card No. 89-0510), respectively [38]. This indicates that ZnO has successfully grown on the carbon cloth. The XRD pattern of CC/Ag<sub>3</sub>PO<sub>4</sub> shows diffraction peaks corresponding to both carbon fiber and Ag<sub>3</sub>PO<sub>4</sub> (JCPDS card No. 74-1876, labeled with  $\blacktriangledown$ ) [39]. As for the CC/ZnO@Ag<sub>3</sub>PO<sub>4</sub> composite, its XRD pattern displays strong diffraction peaks of Ag<sub>3</sub>PO<sub>4</sub> and extremely weak diffraction peaks of ZnO, which is probably due to the full coverage of ZnO by Ag<sub>3</sub>PO<sub>4</sub>. Meanwhile, the characteristic peak of carbon fiber at  $26^\circ$  is practically unobservable, mainly attributed to the fact that the surface of the carbon fibers was entirely coated by ZnO and Ag<sub>3</sub>PO<sub>4</sub>. In addition, the peak intensity of Ag<sub>3</sub>PO<sub>4</sub> in CC/ZnO@Ag<sub>3</sub>PO<sub>4</sub> is stronger than that in CC/Ag<sub>3</sub>PO<sub>4</sub>. It can be inferred that more Ag<sub>3</sub>PO<sub>4</sub> was deposited on the surface of CC/ZnO than directly on the pure carbon cloth.

### 3.2. Morphology

The morphology of the bare carbon cloth, CC/ZnO, CC/Ag<sub>3</sub>PO<sub>4</sub>, and CC/ZnO@Ag<sub>3</sub>PO<sub>4</sub> was investigated by SEM (Figure 3). The microstructure of the bare carbon cloth consisted of carbon fibers with an average diameter of about 10  $\mu\text{m}$  (Figure 3a). A high-magnification SEM image showed that the surface of the carbon fiber was relatively smooth, with wrinkles parallel to the direction of the fibers (Figure 3b). After solvothermal treatment in the precursor solution of ZnO, the carbon fibers became brushy, and many nanowires were found to grow evenly on the surface (Figure 3c). More detailed observation revealed that these ZnO nanowires were crisscross-distributed on the carbon fibers with diameters of 60–160 nm and lengths of more than 2  $\mu\text{m}$  (Figure 3d). The ZnO nanowires with a crisscross structure tended to have high specific surface areas that were available for the deposition of more catalyst particles or adsorption of target molecules. As expected, the surface of CC/ZnO was completely covered by a large number of particles after the deposition of Ag<sub>3</sub>PO<sub>4</sub> (Figure 3e). Further observation of the CC/ZnO@Ag<sub>3</sub>PO<sub>4</sub> composite showed that these Ag<sub>3</sub>PO<sub>4</sub> particles have a polyhedral shape with sizes of 300 nm to 1  $\mu\text{m}$  (Figure 3f). Meanwhile, the ZnO nanowires can be hardly seen in Figure 3f, probably because they were entirely encased by the Ag<sub>3</sub>PO<sub>4</sub> particles. In contrast, it is evident from Figure 3g,h

that only a small quantity of  $\text{Ag}_3\text{PO}_4$  particles are sparsely distributed on the surface of the carbon fibers in  $\text{CC}/\text{Ag}_3\text{PO}_4$ , owing to the relatively smooth surfaces of carbon fibers. The mass loading of  $\text{ZnO}@Ag_3PO_4$  and pure  $\text{Ag}_3\text{PO}_4$  on the carbon cloth was  $7.8 \times 10^{-3}$  and  $1.8 \times 10^{-3}$  g/cm<sup>2</sup>, respectively. The above results are in good correspondence with the XRD analysis.

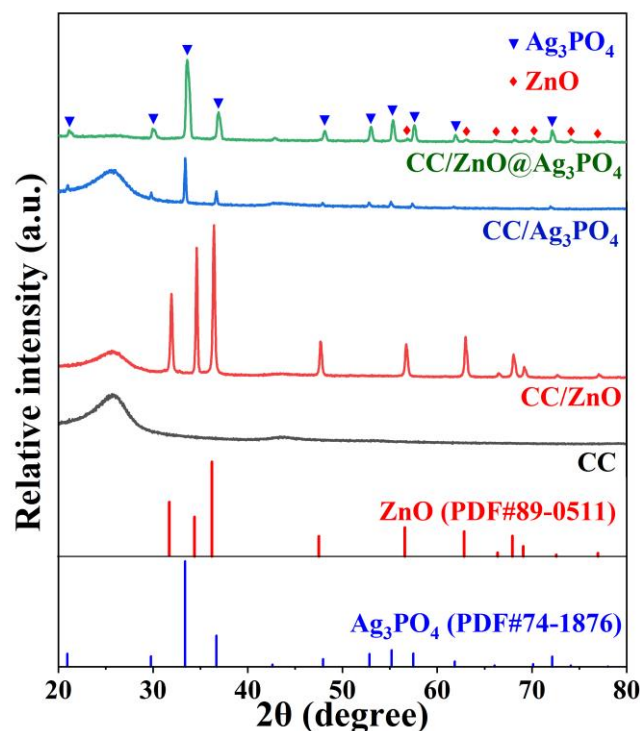


Figure 2. XRD patterns of the CC, CC/ZnO, CC/Ag<sub>3</sub>PO<sub>4</sub>, and CC/ZnO@Ag<sub>3</sub>PO<sub>4</sub> composites.

In order to further investigate the presence of ZnO nanowires in the  $\text{CC}/\text{ZnO}@Ag_3\text{PO}_4$  composite, a control experiment was carried out by shortening the repeated soaking times of  $\text{CC}/\text{ZnO}$  in  $\text{AgNO}_3$  and  $(\text{NH}_4)_2\text{HPO}_4$  solutions to 15 times, and the SEM image of the as-obtained  $\text{CC}/\text{ZnO}@Ag_3\text{PO}_4$  composite is shown in Figure 4a. Obviously, many nanoparticles aggregated on the surfaces of ZnO nanowires (marked by the dotted circle). The diameter of these  $\text{ZnO}@Ag_3\text{PO}_4$  nanowires was about 200 nm. In addition, the  $\text{ZnO}@Ag_3\text{PO}_4$  nanowires were scraped off from the surfaces of carbon fibers for TEM characterization to further confirm the existence of ZnO nanowires. As shown in Figure 4b, the nanowires (dark) were completely covered by many nanoparticles (light) with sizes of about 75 nm, forming a core–shell structure. Additionally, bigger polyhedral particles were found to be adjacent to these nanoparticles. The TEM image is well consistent with the SEM observations in Figure 4a. Furthermore, the elemental mappings of the Ag, Zn, P, and O elements also support the core–shell structure of the  $\text{CC}/\text{ZnO}@Ag_3\text{PO}_4$  composite (Figure 4c). The Zn element only exists in the core nanowires, while the Ag, P, and O elements are distributed near the ZnO nanowires but cover a larger extent. Such tight contact between ZnO and  $\text{Ag}_3\text{PO}_4$  is conducive to the transfer of charge carriers.

### 3.3. Surface Chemistry

The surface composition and chemical states of  $\text{CC}/\text{ZnO}$ ,  $\text{CC}/\text{Ag}_3\text{PO}_4$ , and  $\text{CC}/\text{ZnO}@Ag_3\text{PO}_4$  were further determined by XPS, and the obtained spectra are shown in Figure 5. The full-scanned spectrum of  $\text{CC}/\text{ZnO}@Ag_3\text{PO}_4$  indicates the presence of the Zn, Ag, O, P, and C elements (Figure 5a), which originated from the ternary composites containing carbon fiber, ZnO, and  $\text{Ag}_3\text{PO}_4$ . A close look at the full spectra reveals that the C 1s peak intensity of  $\text{CC}/\text{Ag}_3\text{PO}_4$  is much stronger than that of  $\text{CC}/\text{ZnO}$  and  $\text{CC}/\text{ZnO}@Ag_3\text{PO}_4$ , owing to the low loading of  $\text{Ag}_3\text{PO}_4$  on the pure carbon cloth, which results in a larger fraction of

surface-exposed carbon fibers. This result is in good agreement with the XRD analysis. The high-resolution XPS spectrum of Ag 3d in CC/Ag<sub>3</sub>PO<sub>4</sub> centered at 374.0 and 368.0 eV (Figure 5b), corresponding to the Ag 3d<sub>3/2</sub> and Ag 3d<sub>5/2</sub> core levels of Ag<sup>+</sup>, respectively [34]. Meanwhile, the Ag 3d peaks in CC/ZnO@Ag<sub>3</sub>PO<sub>4</sub> exhibited a positive shift by 0.6 eV compared with those for CC/Ag<sub>3</sub>PO<sub>4</sub>, reflecting an increase in the electron density around the Ag ions (corresponding to a lower formal charge) [40,41], which likely came from the transfer of electrons from ZnO to Ag<sub>3</sub>PO<sub>4</sub>. The characteristic peaks of Zn 2p appeared at 1023.0 and 1046.1 eV (Figure 5c), which correspond to Zn 2p<sub>3/2</sub> and Zn 2p<sub>1/2</sub>, indicating the existence of Zn<sup>2+</sup> from ZnO [42]. The O 1s peak of CC/ZnO could be fitted into three peaks, as shown in Figure 5d. The dominant peak at 530.2 eV was from the Zn–O bonding of ZnO, and the other two peaks at 531.1 and 532.8 eV were associated with dissociatively adsorbed water (Zn–OH) and physically adsorbed H<sub>2</sub>O molecules, respectively [43,44]. For CC/Ag<sub>3</sub>PO<sub>4</sub>, the O 1s XPS spectrum could also be deconvoluted into three peaks at 530.0, 531.6, and 532.6 eV, which are related to the lattice oxygen of Ag<sub>3</sub>PO<sub>4</sub>, chemisorbed oxygen of surface –OH group, and physically adsorbed H<sub>2</sub>O molecules [45–47]. The high-resolution XPS spectrum of O 1s in CC/ZnO@Ag<sub>3</sub>PO<sub>4</sub> could be disintegrated into four peaks. The two peaks at lower binding energy (529.9 and 530.7 eV) are assigned to the lattice oxygen of Ag<sub>3</sub>PO<sub>4</sub> and Zn–O bonding of ZnO [48,49], respectively. The other two peaks at higher binding energy (531.5 and 532.4 eV) are related to the surface –OH group and H<sub>2</sub>O molecules adsorbed on the surface of the CC/ZnO@Ag<sub>3</sub>PO<sub>4</sub> composite [50]. The slight shift of O 1s peaks related to Zn–O and Ag–O in the CC/ZnO@Ag<sub>3</sub>PO<sub>4</sub> composite was observed, compared with O 1s peaks in CC/ZnO and CC/Ag<sub>3</sub>PO<sub>4</sub>, implying the formation of chemical bonding between ZnO and Ag<sub>3</sub>PO<sub>4</sub>. The above XPS results further confirmed the successful synthesis of a CC/ZnO@Ag<sub>3</sub>PO<sub>4</sub> composite photocatalyst.

### 3.4. Photocatalytic Dye Removal Performance

The photocatalytic activities of the prepared samples for the removal of RhB from an aqueous solution were performed under visible light from LED lamp irradiation. As can be seen from Figure 7a, only a small amount of RhB was adsorbed for all samples in the dark conditions. The CC/ZnO sample exhibited weak photocatalytic activity, with only about 15.4% removal achieved after 100 min of light illumination. The CC/Ag<sub>3</sub>PO<sub>4</sub> sample also exhibited a modest photocatalytic performance, with 35.3% RhB removal. By contrast, 87.1% of RhB was degraded by the CC/ZnO@Ag<sub>3</sub>PO<sub>4</sub> composite, which showed the highest photocatalytic activity with a reaction rate constant of 0.0191 min<sup>−1</sup>, exceeding that of CC/Ag<sub>3</sub>PO<sub>4</sub> by 4.8 times and that of CC/ZnO by a factor of 15.9 (Figure 7b). The stability and reusability are essential to the practical application of the photocatalysts. Herein, three cycles of photocatalytic experiments were carried out to investigate the photocatalytic stability of CC/ZnO@Ag<sub>3</sub>PO<sub>4</sub> and CC/Ag<sub>3</sub>PO<sub>4</sub>. The RhB removal ratio for the CC/ZnO@Ag<sub>3</sub>PO<sub>4</sub> composite was 30.9% after three cycle tests (Figure 7c), showing a 64.5% activity loss compared with its performance in the first test. However, only 4.7% of the decomposition ratio of RhB remained for CC/Ag<sub>3</sub>PO<sub>4</sub> after three cycles of photocatalytic degradation tests (Figure 7d), which exhibited an 88.0% activity loss compared with itself. These results indicated that the heterostructure formed between ZnO and Ag<sub>3</sub>PO<sub>4</sub> is beneficial to the improvement of photocatalytic activity and stability of the CC/ZnO@Ag<sub>3</sub>PO<sub>4</sub> composite.

### 3.5. Optical Absorption Property

The UV–Visible DRS test was carried out to explore the optical absorption of CC, CC/ZnO, CC/Ag<sub>3</sub>PO<sub>4</sub>, CC/ZnO@Ag<sub>3</sub>PO<sub>4</sub>, and pure Ag<sub>3</sub>PO<sub>4</sub> powder, and the results are shown in Figure 6. It can be found that the dark grey CC has a strong light absorption within the entire UV–visible light region examined. The CC/ZnO exhibited strong absorption in the ultraviolet light region of 200–400 nm, and its relatively strong absorption in the visible light region was brought about by the carbon cloth. The intrinsic absorption edge of pure Ag<sub>3</sub>PO<sub>4</sub> powder is about 536.5 nm, corresponding to a bandgap energy of 2.31 eV. The

CC/ZnO@Ag<sub>3</sub>PO<sub>4</sub> also displayed a similar light absorption curve to that of pure Ag<sub>3</sub>PO<sub>4</sub>, except for an enhanced absorption in the 470–800 nm region, possibly because the unique structure of the ZnO nanowires grown on carbon fibers enhanced light scattering. This can also be verified from the relatively strong absorption of CC/ZnO in the visible light region. In addition, the light absorbance of CC/Ag<sub>3</sub>PO<sub>4</sub> is higher than that of CC/ZnO@Ag<sub>3</sub>PO<sub>4</sub>, which can be attributed to the fact that the quantity of Ag<sub>3</sub>PO<sub>4</sub> particles directly deposited on the surface of the carbon cloth was much less than that deposited on CC/ZnO, leading to more exposed carbon fibers in CC/Ag<sub>3</sub>PO<sub>4</sub> than in CC/ZnO@Ag<sub>3</sub>PO<sub>4</sub>. It is well known that the dark grey carbon fibers can almost absorb all the light. The above results also match well with the XRD and SEM analyses.

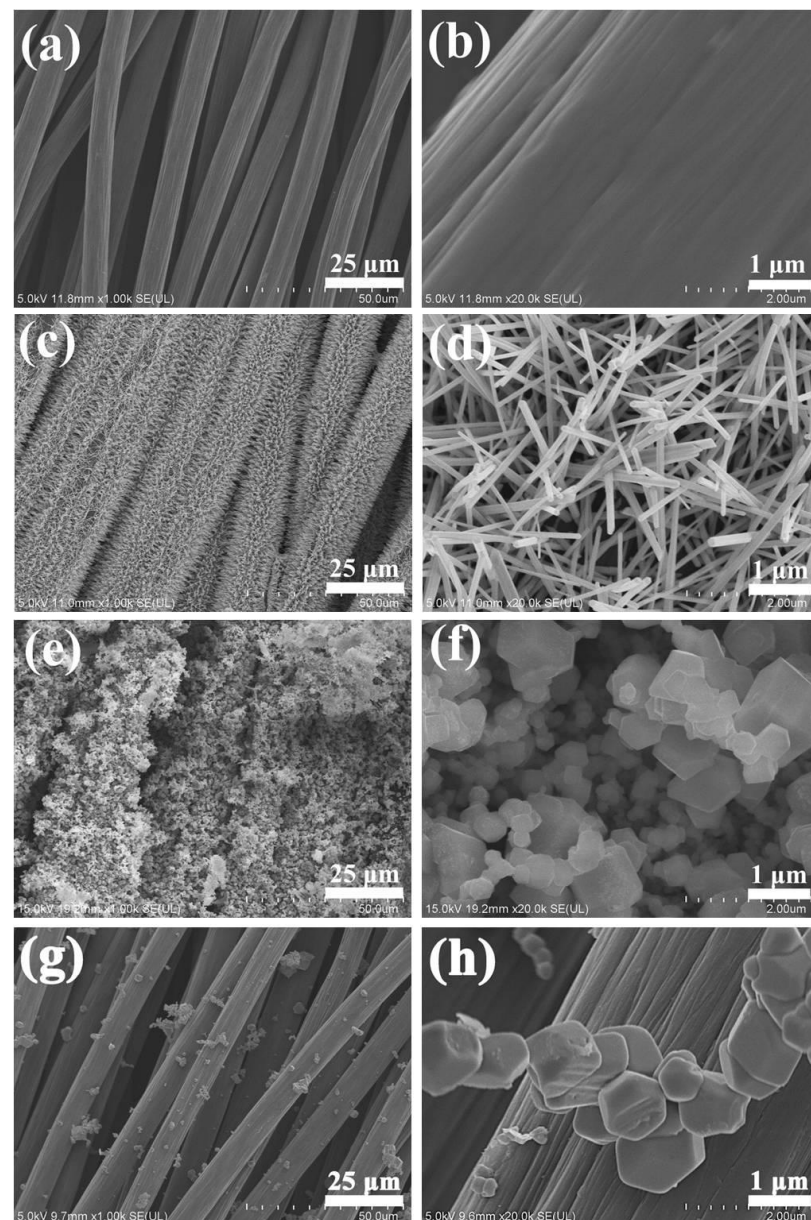


**Figure 3.** SEM images of CC (a,b), CC/ZnO (c,d), CC/ZnO@Ag<sub>3</sub>PO<sub>4</sub> (e,f), and CC/Ag<sub>3</sub>PO<sub>4</sub> (g,h).

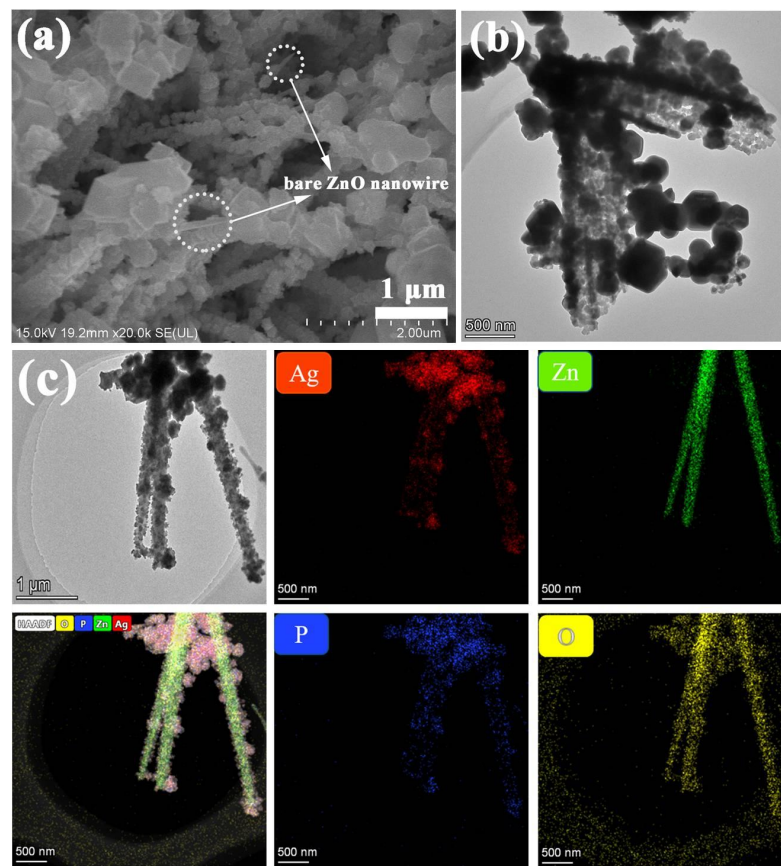


Figure 4. SEM image (a), TEM image, (b) and corresponding elemental mappings (c) of the CC/ZnO@Ag<sub>3</sub>PO<sub>4</sub> composite, which show distribution of the Ag, Zn, P, and O elements.

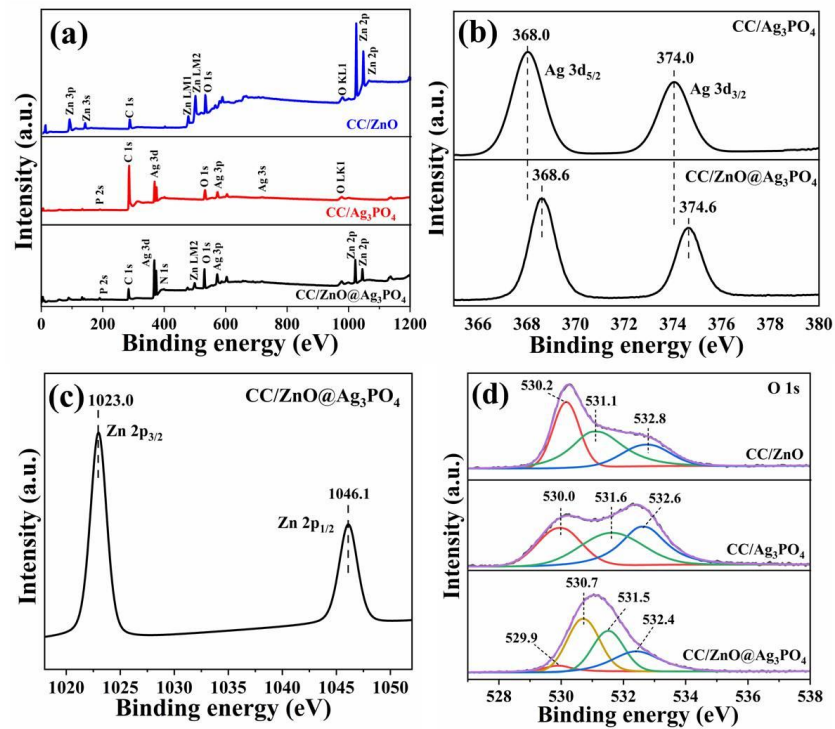


Figure 5. XPS survey spectrum (a) and high-resolution XPS spectra of Ag 3d (b), Zn 2p (c), O 1s (d) of CC/ZnO, CC/Ag<sub>3</sub>PO<sub>4</sub>, and the CC/ZnO@Ag<sub>3</sub>PO<sub>4</sub> composite.

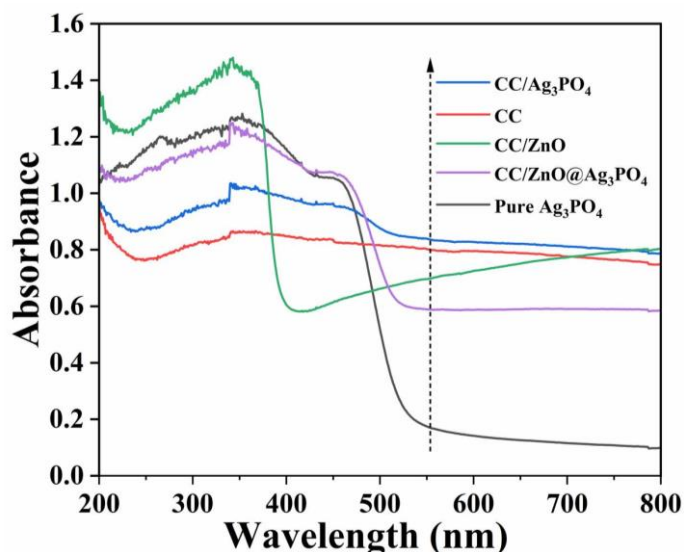


Figure 6. UV-Vis diffuse reflectance spectra of the as-prepared samples.

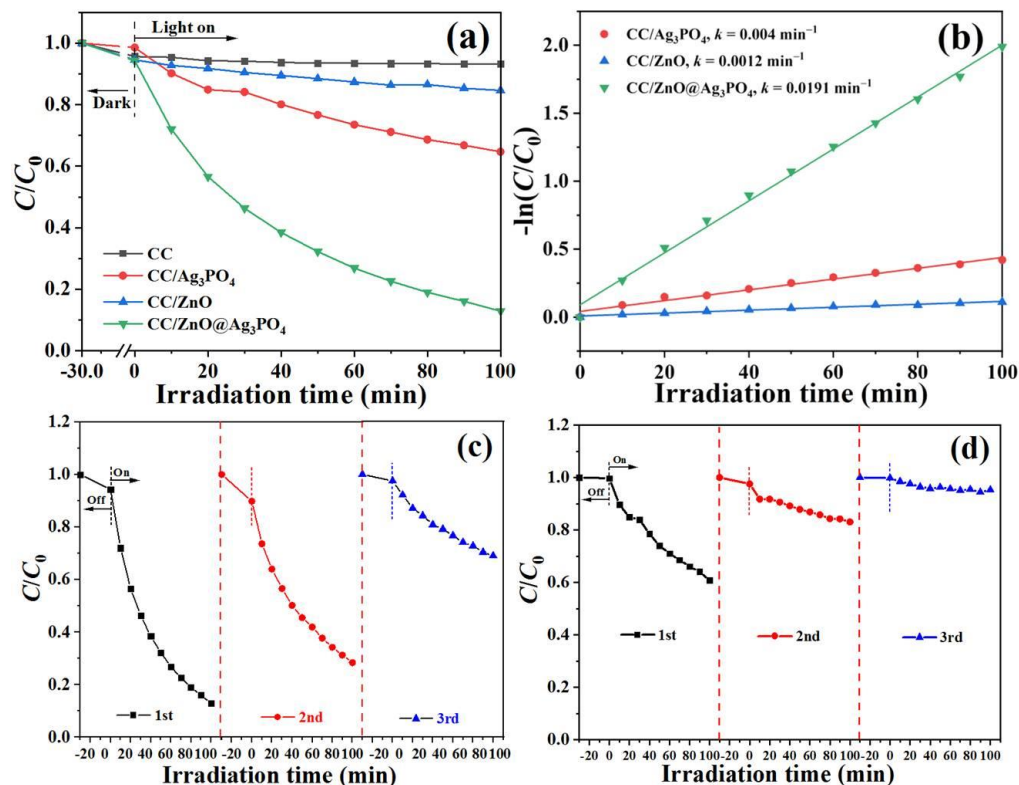


Figure 7. Comparison of the photocatalytic activities (a) and apparent reaction rate constants (b) of CC, CC/ZnO, CC/ZnO@Ag<sub>3</sub>PO<sub>4</sub>, and CC/Ag<sub>3</sub>PO<sub>4</sub> for the degradation of RhB under visible light irradiation, and photocatalytic recyclability of the CC/ZnO@Ag<sub>3</sub>PO<sub>4</sub> composite (c) and CC/Ag<sub>3</sub>PO<sub>4</sub> (d).

#### 4. Possible Photocatalytic Mechanism

On the basis of the above results and the literature, a possible charge separation and transfer mechanism for the enhanced activity and stability of the CC/ZnO@Ag<sub>3</sub>PO<sub>4</sub> composite was proposed (Figure 8). According to the literature, ZnO possesses a more negative valence band (VB) and conduction band (CB) edge than that of Ag<sub>3</sub>PO<sub>4</sub> [51]. When they come into contact with each other, electrons transfer from ZnO to Ag<sub>3</sub>PO<sub>4</sub>, and an internal electric field (IEF) is created at the interface of ZnO and Ag<sub>3</sub>PO<sub>4</sub> [52]. The

direction of the IEF points from ZnO to  $\text{Ag}_3\text{PO}_4$ , as marked by the arrow in Figure 8. Under visible light excitation, ZnO shows weak photocatalytic activity, probably due to its intrinsic defect in the crystal and inefficient light absorption [53]. Simultaneously, both ZnO and  $\text{Ag}_3\text{PO}_4$  can be excited, and the electrons in the VB leap into the CB, while the positively charged holes ( $\text{h}^+$ ) are left in the VB. Subsequently, the photogenerated electrons in the CB of  $\text{Ag}_3\text{PO}_4$  shift towards ZnO, as driven by the interfacial IEF, and recombine with the  $\text{h}^+$  in the VB of ZnO. Apparently, an S-scheme mechanism applies well to the heterojunction between  $\text{Ag}_3\text{PO}_4$  and ZnO, and the transfer of electrons and holes in the IEF region follows a slide-like pathway. Benefitting from this ZnO@ $\text{Ag}_3\text{PO}_4$  S-scheme heterojunction, the photogenerated charges efficiently separate. Consequently, the holes are enriched in the VB of  $\text{Ag}_3\text{PO}_4$ , while the electrons are enriched in the CB of ZnO. It has been reported that the  $\text{h}^+$  and superoxide anion radicals ( $\cdot\text{O}_2^-$ ) are the main active species in the ZnO/ $\text{Ag}_3\text{PO}_4$  reaction system, according to the free radical capture experiment [54,55]. The holes reserving high oxidation ability in the VB of  $\text{Ag}_3\text{PO}_4$  can directly participate in the degradation of RhB. In addition, it is well known that the carbon fibers with a one-dimensional linear structure possess excellent electrical conductivity, which rapidly receive electrons from the CB of ZnO. Then, the dissolved oxygen molecules are captured by the electrons enriched in the carbon fibers and reduced into  $\cdot\text{O}_2^-$  radicals, which further degrade RhB molecules into  $\text{CO}_2$ ,  $\text{H}_2\text{O}$ , and small molecular compounds [35]. Moreover, the ZnO nanowires directly grown on the conductive carbon fibers ensure good adhesion of the ZnO@ $\text{Ag}_3\text{PO}_4$  core-shell structure with the carbon cloth substrate.

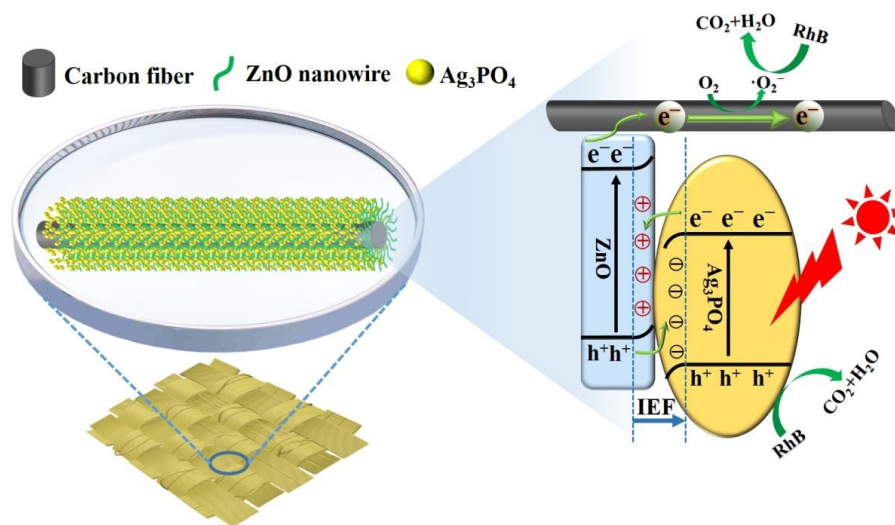


Figure 8. Schematic diagram for the improved charge separation of the CC/ZnO@ $\text{Ag}_3\text{PO}_4$  composite.

## 5. Conclusions

In summary, the carbon cloth-supported ZnO@ $\text{Ag}_3\text{PO}_4$  composite with a core-shell structure was successfully prepared by a two-step process including a solvothermal method and a succeeding impregnation-deposition method. The as-prepared CC/ZnO@ $\text{Ag}_3\text{PO}_4$  displayed an enhanced photocatalytic activity for degrading RhB under visible light irradiation compared with that of CC/ZnO and CC/ $\text{Ag}_3\text{PO}_4$ , mainly attributed to the synergistic effect of the carbon cloth, ZnO, and  $\text{Ag}_3\text{PO}_4$ . The construction of a S-scheme heterojunction between ZnO and  $\text{Ag}_3\text{PO}_4$  was mainly responsible for the enhanced activity of the composite, which suppressed the recombination of the charge carriers within ZnO or  $\text{Ag}_3\text{PO}_4$  itself by transferring electrons from the CB of  $\text{Ag}_3\text{PO}_4$  to the VB of ZnO through the internal electric field. Additionally, carbon fibers further accelerated the transmission of electrons; therefore, the charge separation efficiency was further improved. The carbon cloth-supported ZnO@ $\text{Ag}_3\text{PO}_4$  can be easily separated from the solution and repeatedly used, demonstrating a fair recyclability and potential in practical applications. Neverthe-

less, the decreased activity of CC/ZnO@Ag<sub>3</sub>PO<sub>4</sub> after many cycles of photocatalytic tests still needs to be further explored.

**Author Contributions:** Conceptualization, W.W. and C.J.; sample preparation, Y.Y., Q.G., S.J. and H.L.; sample characterization, Y.Y. and Q.G.; photocatalytic test, Y.Y., Q.G. and S.J.; writing—original draft preparation, Y.Y.; writing—review and editing, W.W. and C.J.; supervision, W.W.; project administration, L.W. and H.Z.; and funding acquisition, W.W., C.J. and L.W. All authors have read and agreed to the published version of the manuscript.

**Funding:** This research was funded by the National Natural Science Foundation of China (grant numbers 52072079 and 51802305), the Natural Science Foundation of Guangdong Province, China (No. 2021A1515010445), and the Fundamental Research Funds for the Central Universities of Nankai University.

**Institutional Review Board Statement:** Not applicable.

**Informed Consent Statement:** Not applicable.

**Data Availability Statement:** All the data are available within the manuscript.

**Conflicts of Interest:** The authors declare no conflict of interest. The funders had no role in the design of the study; in the collection, analyses, or interpretation of the data; in the writing of the manuscript; or in the decision to publish the results.

## References

1. Dire, D.J.; Wilkinson, J.A. Acute exposure to rhodamine B. *J. Toxicol. Clin. Toxicol.* **1987**, *25*, 603–607. [\[CrossRef\]](#)
2. Verma, Y. Acute toxicity assessment of textile dyes and textile and dye industrial effluents using *Daphnia magna* bioassay. *Toxicol. Ind. Health* **2008**, *24*, 491–500.
3. Fernández, C.; Larrechi, M.S.; Callao, M.P. An analytical overview of processes for removing organic dyes from wastewater effluents. *TrAC Trends Anal. Chem.* **2010**, *29*, 1202–1211. [\[CrossRef\]](#)
4. Shanker, U.; Rani, M.; Jassal, V. Degradation of hazardous organic dyes in water by nanomaterials. *Environ. Chem. Lett.* **2017**, *15*, 623–642. [\[CrossRef\]](#)
5. Loc, N.X.; Tuyen, P.T.T.; Mai, L.C.; Phuong, D.T.M. Chitosan-modified biochar and unmodified biochar for methyl orange: Adsorption characteristics and mechanism exploration. *Toxics* **2022**, *10*, 500. [\[CrossRef\]](#)
6. Gomaa, H.; El-Monaem, E.M.A.; Eltaweil, A.S.; Omer, A.M. Efficient removal of noxious methylene blue and crystal violet dyes at neutral conditions by reusable montmorillonite/NiFe<sub>2</sub>O<sub>4</sub>@amine-functionalized chitosan composite. *Sci. Rep.* **2022**, *12*, 15499. [\[CrossRef\]](#)
7. Jaleel, R.M.; Uc, J.R.; Pinheiro, D.; NK, R.; Devi KR, S.; Park, J.; Manickam, S.; Choi, M.Y. Architecture of visible-light induced Z-scheme MoS<sub>2</sub>/g-C<sub>3</sub>N<sub>4</sub>/ZnO ternary photocatalysts for malachite green dye degradation. *Environ. Res.* **2022**, *214*, 113742.
8. Chu, M.N.; Nguyen, L.T.H.; Truong, M.X.; Do, H.T.; Duong, T.T.A.; Nguyen, L.T.T.; Pham, M.A.; Tran, T.K.N.; Ngo, T.C.Q.; Pham, V.H. Ce<sup>3+</sup>/Ce<sup>4+</sup>-Doped ZrO<sub>2</sub>/CuO nanocomposite for enhanced photocatalytic degradation of methylene blue under visible light. *Toxics* **2022**, *10*, 463. [\[CrossRef\]](#)
9. Gomaa, H.; Hussein, M.A.T.; Motawea, M.M.; Aboraia, A.M.; Cheira, M.F.; Alotaibi, M.T.; El-Bahy, S.M.; Ali, H.M. A hybrid mesoporous CuO@barley straw-derived SiO<sub>2</sub> nanocomposite for adsorption and photocatalytic degradation of methylene blue from real wastewater. *Colloids Surf. A* **2022**, *644*, 128811. [\[CrossRef\]](#)
10. Motawea, M.M.; Hussein, M.A.T.; Elsenety, M.M.; Ali, H.M.; El-Nasr, T.A.S.; Gomaa, H. Mesoporous hierarchical ZrO<sub>2</sub>@rice straw-derived SiO<sub>2</sub> nanocomposite for rapid adsorption and sunlight-driven photocatalytic degradation of methylene blue. *J. Photochem. Photobiol. A* **2022**, *426*, 113758. [\[CrossRef\]](#)
11. Chang, J.S.; Strunk, J.; Chong, M.N.; Poh, P.E.; Ocon, J.D. Multi-dimensional zinc oxide (ZnO) nanoarchitectures as efficient photocatalysts: What is the fundamental factor that determines photoactivity in ZnO. *J. Hazard. Mater.* **2020**, *381*, 120958. [\[CrossRef\]](#)
12. Lam, S.M.; Sin, J.C.; Abdullah, A.Z.; Mohamed, A.R. Degradation of wastewaters containing organic dyes photocatalysed by zinc oxide: A review. *Desalin. Water Treat.* **2012**, *41*, 131–169. [\[CrossRef\]](#)
13. Biglar, F.; Talaiekhosani, A.; Aminsharei, F.; Park, J.; Baighi, A.; Rezaia, S. Application of ZnO-Nd nano-photocatalyst for the reactive red 198 dye decolorization in the falling-film photocatalytic reactor. *Toxics* **2021**, *9*, 254. [\[CrossRef\]](#)
14. Kassem, K.O.; Hussein, M.A.T.; Motawea, M.M.; Gomaa, H.; Alrowaili, Z.A.; Ezzeldien, M. Design of mesoporous ZnO @ silica fume-derived SiO<sub>2</sub> nanocomposite as photocatalyst for efficient crystal violet removal: Effective route to recycle industrial waste. *J. Clean. Prod.* **2021**, *326*, 129416. [\[CrossRef\]](#)
15. Zhang, L.W.; Cheng, H.Y.; Zong, R.L.; Zhu, Y.F. Photocorrosion suppression of ZnO nanoparticles via hybridization with graphite-like carbon and enhanced photocatalytic activity. *J. Phys. Chem. C* **2009**, *113*, 2368–2374. [\[CrossRef\]](#)

16. Jiang, C.J.; Aiken, G.R.; Hsu-Kim, H. Effects of natural organic matter properties on the dissolution kinetics of zinc oxide nanoparticles. *Environ. Sci. Technol.* **2015**, *49*, 11476–11484. [[CrossRef](#)]
17. Kumar, S.G.; Rao, K.S.R.K. Zinc oxide based photocatalysis: Tailoring surface-bulk structure and related interfacial charge carrier dynamics for better environmental applications. *RSC Adv.* **2015**, *5*, 3306–3351. [[CrossRef](#)]
18. Zhu, B.C.; Xia, P.F.; Li, Y.; Ho, W.K.; Yu, J.G. Fabrication and photocatalytic activity enhanced mechanism of direct Z-scheme g-C<sub>3</sub>N<sub>4</sub>/Ag<sub>2</sub>WO<sub>4</sub> photocatalyst. *Appl. Surf. Sci.* **2017**, *391*, 175–183. [[CrossRef](#)]
19. Xiao, T.T.; Tang, Z.; Yang, Y.; Tang, L.P.; Zhou, Y.; Zou, Z.G. In situ construction of hierarchical WO<sub>3</sub>/g-C<sub>3</sub>N<sub>4</sub> composite hollow microspheres as a Z-scheme photocatalyst for the degradation of antibiotics. *Appl. Catal. B* **2018**, *220*, 417–428. [[CrossRef](#)]
20. Yang, X.B.; Hu, J.P.; Pan, J.J.; Shen, Y.B.; Cheng, K.J. Fabrication of Ag/ZnO@N-carbon core@shell photocatalyst for efficient photocatalytic degradation of rhodamine B. *Front. Chem.* **2022**, *10*, 950007. [[CrossRef](#)]
21. Yi, Z.G.; Ye, J.H.; Kikugawa, N.; Kako, T.; Ouyang, S.X.; Williams, H.S.; Yang, H.; Cao, J.Y.; Luo, W.J.; Li, Z.S.; et al. An orthophosphate semiconductor with photooxidation properties under visible-light irradiation. *Nat. Mater.* **2010**, *9*, 559–564. [[CrossRef](#)]
22. Liu, Y.; Wang, W.G.; Si, M.Z.; Yu, Y.F.; Zhang, H.Y. (Yb<sup>3+</sup>, Er<sup>3+</sup>) co-doped TiO<sub>2</sub>/Ag<sub>3</sub>PO<sub>4</sub> hybrid photocatalyst with enhanced activity for photodegradation of phenol. *Appl. Surf. Sci.* **2019**, *463*, 159–168. [[CrossRef](#)]
23. Dong, P.Y.; Huo, G.H.; Liu, C.; Zhang, X.J.; Tian, H.; Xu, F.H.; Xi, X.G.; Shao, R. Origin of activity and stability enhancement for Ag<sub>3</sub>PO<sub>4</sub> photocatalyst after calcination. *Materials* **2016**, *9*, 968. [[CrossRef](#)]
24. Wang, W.G.; Cheng, B.; Yu, J.G.; Liu, G.; Fan, W.H. Visible-light photocatalytic activity and deactivation mechanism of Ag<sub>3</sub>PO<sub>4</sub> spherical particles. *Chem.-Asian J.* **2012**, *7*, 1902–1908. [[CrossRef](#)]
25. Dong, C.; Wu, K.L.; Li, M.R.; Liu, L.; Wei, X.W. Synthesis of Ag<sub>3</sub>PO<sub>4</sub>-ZnO nanorod composites with high visible-light photocatalytic activity. *Catal. Commun.* **2014**, *46*, 32–35. [[CrossRef](#)]
26. Liu, W.; Wang, M.L.; Xu, C.X.; Chen, S.F.; Fu, X.L. Ag<sub>3</sub>PO<sub>4</sub>/ZnO: An efficient visible-light-sensitized composite with its application in photocatalytic degradation of rhodamine B. *Mater. Res. Bull.* **2013**, *48*, 106–113. [[CrossRef](#)]
27. Yi, Z.; Li, X.; Wu, H.; Chen, X.F.; Yang, H.; Tang, Y.J.; Yi, Y.G.; Wang, J.Q.; Wu, P.H. Fabrication of ZnO@Ag<sub>3</sub>PO<sub>4</sub> core-shell nanocomposite arrays as photoanodes and their photoelectric properties. *Nanomaterials* **2019**, *9*, 1254. [[CrossRef](#)]
28. Zhong, J.B.; Li, J.Z.; Wang, T.; Zeng, J.; Si, Y.J.; Cheng, C.Z.; Li, M.J.; Wang, P.; Ding, J. Improved solar-driven photocatalytic performance of Ag<sub>3</sub>PO<sub>4</sub>/ZnO composites benefiting from enhanced charge separation with a typical Z-scheme mechanism. *Appl. Phys. A Mater. Sci. Process.* **2016**, *122*, 4. [[CrossRef](#)]
29. Si, M.Z.; Wang, W.G.; Guan, Q.F.; Zhang, H.Y.; Puttaswamy, M. Facile fabrication of highly catalytic-active Ag<sub>2</sub>CO<sub>3</sub>/AgBr/graphene oxide ternary composites towards the photocatalytic wastewater treatment. *Environ. Sci. Pollut. Res.* **2021**, *28*, 4173–4183. [[CrossRef](#)]
30. Xie, Y.; Luo, S.Q.; Huang, H.W.; Huang, Z.H.; Liu, Y.G.; Fang, M.H.; Wu, X.W.; Min, X. Construction of an Ag<sub>3</sub>PO<sub>4</sub> morphological homojunction for enhanced photocatalytic performance and mechanism investigation. *Colloids Surf. A* **2018**, *546*, 99–106. [[CrossRef](#)]
31. Hussein, M.A.T.; Motawea, M.M.; Elsenety, M.M.; El-Bahy, S.M.; Gomaa, H. Mesoporous spongy Ni-Co oxides@wheat straw-derived SiO<sub>2</sub> for adsorption and photocatalytic degradation of methylene blue pollutants. *Appl. Nanosci.* **2022**, *12*, 1519–1536. [[CrossRef](#)]
32. Yao, Y.; Dong, W.B.; Zhao, Z.; Cui, H.N.; Liao, G.L. Vertically aligned 1T-WS<sub>2</sub> nanosheets supported on carbon cloth as a high-performance flexible photocatalyst. *Colloids Surf. A* **2022**, *649*, 129533. [[CrossRef](#)]
33. Chen, H.H.; Deng, L.B.; Luo, S.; Ren, X.Z.; Li, Y.L.; Sun, L.N.; Zhang, P.X.; Chen, G.Q.; Gao, Y. Flexible three-dimensional heterostructured ZnO-Co<sub>3</sub>O<sub>4</sub> on carbon cloth as free-standing anode with outstanding Li/Na storage performance. *J. Electrochem. Soc.* **2018**, *165*, A3932–A3942. [[CrossRef](#)]
34. Meng, S.J.; Hong, Y.; Dai, Z.Y.; Huang, W.; Dong, X.C. Simultaneous detection of dihydroxybenzene isomers with ZnO nanorod/carbon cloth electrodes. *ACS Appl. Mater. Interfaces* **2017**, *9*, 12453–12460. [[CrossRef](#)]
35. Liu, Y.; Wang, W.G.; Si, M.Z.; Zhang, H.Y. Carbon cloth-supported MoS<sub>2</sub>/Ag<sub>2</sub>S/Ag<sub>3</sub>PO<sub>4</sub> composite with high photocatalytic activity and recyclability. *ChemCatChem* **2019**, *11*, 1017–1025.
36. Skjolding, L.M.; Jorgensen, L.v.G.; Dyhr, K.S.; Koppl, C.J.; McKnight, U.S.; Bauer-Gottwein, P.; Mayer, P.; Bjerg, P.L.; Baun, A. Assessing the aquatic toxicity and environmental safety of tracer compounds Rhodamine B and Rhodamine WT. *Water Res.* **2021**, *197*, 117109. [[CrossRef](#)]
37. Yan, Y.P.; Wang, B.; Yan, C.Z.; Kang, D.J. Decorating ZnO nanoflakes on carbon cloth: Free-standing, highly stable lithium-ion battery anodes. *Ceram. Int.* **2019**, *45*, 15906–15912. [[CrossRef](#)]
38. Ashkarran, A.A.; Irajizad, A.; Mahdavi, S.M.; Ahadian, M.M. ZnO nanoparticles prepared by electrical arc discharge method in water. *Mater. Chem. Phys.* **2009**, *118*, 6–8. [[CrossRef](#)]
39. Li, W.; Qin, L.; Wang, Z.H.; Xu, G.C.; Zheng, H.C.; Zhou, L.M.; Chen, Z.Q. Efficient porous carbon nitride/Ag<sub>3</sub>PO<sub>4</sub> photocatalyst for selective oxidation of amines to imines: Z-scheme heterojunction and interfacial adsorption. *Colloids Surf. A* **2022**, *652*, 129806. [[CrossRef](#)]
40. Liu, Y.P.; Fang, L.; Lu, H.D.; Liu, L.J.; Wang, H.; Hu, C.Z. Highly efficient and stable Ag/Ag<sub>3</sub>PO<sub>4</sub> plasmonic photocatalyst in visible light. *Catal. Commun.* **2012**, *17*, 200–204. [[CrossRef](#)]

41. Cao, J.; Luo, B.D.; Lin, H.L.; Xu, B.Y.; Chen, S.F. Visible light photocatalytic activity enhancement and mechanism of AgBr/Ag<sub>3</sub>PO<sub>4</sub> hybrids for degradation of methyl orange. *J. Hazard. Mater.* **2012**, *217–218*, 107–115. [[CrossRef](#)] [[PubMed](#)]
42. Saravanan, R.; Thirumal, E.; Gupta, V.K.; Narayanan, V.; Stephen, A. The photocatalytic activity of ZnO prepared by simple thermal decomposition method at various temperatures. *J. Mol. Liq.* **2013**, *177*, 394–401. [[CrossRef](#)]
43. Al-Gaashani, R.; Ramiman, S.; Daud, A.R.; Tabet, N.; Al-Douri, Y. XPS and optical studies of different morphologies of ZnO nanostructures prepared by microwave methods. *Ceram. Int.* **2013**, *39*, 2283–2292. [[CrossRef](#)]
44. Tian, Y.Y.; Fang, Q.H.; Li, J. Molecular dynamics simulations for nanoindentation response of nanotwinned FeNiCrCoCu high entropy alloy. *Nanotechnology* **2020**, *31*, 465701. [[CrossRef](#)] [[PubMed](#)]
45. Jin, B.; Zhou, X.S.; Luo, J.; Xu, X.Y.; Ma, L.; Huang, D.Y.; Shao, Z.L.; Luo, Z.H. Fabrication and characterization of high efficiency and stable Ag<sub>3</sub>PO<sub>4</sub>/TiO<sub>2</sub> nanowire array heterostructure photoelectrodes for the degradation of methyl orange under visible light irradiation. *RSC Adv.* **2015**, *59*, 48118–48123. [[CrossRef](#)]
46. Chai, B.; Zou, F.Y.; Chen, W.J. Facile synthesis of Ag<sub>3</sub>PO<sub>4</sub>/C<sub>3</sub>N<sub>4</sub> composites with improved visible light photocatalytic activity. *J. Mater. Res.* **2015**, *30*, 1128–1136. [[CrossRef](#)]
47. Miao, X.L.; Yue, X.Y.; Ji, Z.Y.; Shen, X.P.; Zhou, H.; Liu, M.M.; Xu, K.Q.; Zhu, J.; Zhu, G.X.; Kong, L.R.; et al. Nitrogen-doped carbon dots decorated on g-C<sub>3</sub>N<sub>4</sub>/Ag<sub>3</sub>PO<sub>4</sub> photocatalyst with improved visible light photocatalytic activity and mechanism insight. *Appl. Catal. B* **2018**, *227*, 459–469. [[CrossRef](#)]
48. Naraginti, S.; Yu, Y.Y.; Fang, Z.; Yong, Y.C. Novel tetrahedral Ag<sub>3</sub>PO<sub>4</sub>@N-rGO for photocatalytic detoxification of sulfamethoxazole: Process optimization, transformation pathways and biotoxicity assessment. *Chem. Eng. J.* **2019**, *375*, 122035. [[CrossRef](#)]
49. Choi, J.S.; Jung, R. In-situ XPS study of core-levels of ZnO thin films at the interface with graphene/Cu. *J. Korean Phys. Soc.* **2018**, *73*, 1546–1549. [[CrossRef](#)]
50. Shen, Y.Z.; Zhu, Z.D.; Wang, X.G.; Khan, A.; Gong, J.Y.; Zhang, Y.R. Synthesis of Z-scheme g-C<sub>3</sub>N<sub>4</sub>/Ag/Ag<sub>3</sub>PO<sub>4</sub> composite for enhanced photocatalytic degradation of phenol and selective oxidation of gaseous isopropanol. *Mater. Res. Bull.* **2018**, *107*, 407–415. [[CrossRef](#)]
51. Wang, J.; Xia, Y.; Dong, Y.; Chen, R.S.; Xiang, L.; Komarneni, S. Defect-rich ZnO nanosheets of high surface area as an efficient visible-light photocatalyst. *Appl. Catal. B* **2016**, *192*, 8–16. [[CrossRef](#)]
52. Xu, Q.L.; Zhang, L.Y.; Cheng, B.; Fan, J.J.; Yu, J.G. S-Scheme heterojunction photocatalyst. *Chem* **2020**, *6*, 1543–1559. [[CrossRef](#)]
53. Pan, J.Q.; Zhang, X.F.; Mei, J.; Wang, S.; You, M.Z.; Zheng, Y.Y.; Cui, C.; Li, C.R. The cotton cellulose nanofibers framework of Z-Scheme ZnO/Ag<sub>3</sub>PO<sub>4</sub> heterojunction for visible-light photocatalysis. *J. Mater. Sci. Mater. Electron.* **2017**, *28*, 17744–17749. [[CrossRef](#)]
54. Zhu, P.F.; Duan, M.; Wang, R.X.; Xu, J.; Zou, P.; Jia, H.S. Facile synthesis of ZnO/GO/Ag<sub>3</sub>PO<sub>4</sub> heterojunction photocatalyst with excellent photodegradation activity for tetracycline hydrochloride under visible light. *Colloids Surf. A* **2020**, *602*, 125118. [[CrossRef](#)]
55. Du, C.Y.; Song, J.H.; Tan, S.Y.; Yang, L.; Yu, G.L.; Chen, H.; Zhou, L.; Zhang, Z.; Zhang, Y.; Su, Y.H.; et al. Facile synthesis of Z-scheme ZnO/Ag/Ag<sub>3</sub>PO<sub>4</sub> composite photocatalysts with enhanced performance for the degradation of ciprofloxacin. *Mater. Chem. Phys.* **2021**, *260*, 124136. [[CrossRef](#)]

**Disclaimer/Publisher’s Note:** The statements, opinions and data contained in all publications are solely those of the individual author(s) and contributor(s) and not of MDPI and/or the editor(s). MDPI and/or the editor(s) disclaim responsibility for any injury to people or property resulting from any ideas, methods, instructions or products referred to in the content.